Journal of Sedimentary Research

The geomorphological distribution of subaqueous tufa columns within a hypersaline lake: Mono Lake, USA.

--Manuscript Draft--

Manuscript Number:	2021.034R2
Article Type:	Research Article
Corresponding Author:	Mike Rogerson Northumbria University Drax, County UNITED KINGDOM
First Author:	C.E. Keevil
Order of Authors:	C.E. Keevil
	Mike Rogerson
	M. Rogerson
	D.R. Parsons
	R. Mercedes-Martín
	A.T. Brasier
	J.J.G. Reijmer
	A. Matthews
Abstract:	Understanding the flow of carbon through hyperalkaline lakes is a key means of understanding their biogeochemistry, sedimentology and their palaeoenvironmental and palaeoclimatic records. Furthermore, understanding how mineral precipitation is regulated in these lakes can provide insight into how their carbon sequestration behaviour can be managed. We report geophysical surveys of Mono Lake, California, USA, which show unanticipated geomorphological control on the recent / contemporary formation of lacustrine carbonate formations (“tufa”). Acquired shallow seismic data shows a fault zone below the lake floor, but despite the regional evidence for geothermal waters rising up these fractures, we find no evidence for tufa precipitation at the surface exposure of this structure, either in the seismic data or in the swath bathymetry. However, we do find sub-lacustrine tufa columns in this data elsewhere, which is the first time these have been reported directly. We find and report on a strong link between column location and meteoric Ca supply, with the latter sourced either through surface runoff or groundwater. For example, a region close to a creek inlet has more frequent and larger tufa bodies, which grow at a greater depth range, than another region far from an inlet but close to the fault. This demonstrates the importance of meteoric water ingress in regulating carbonate mineral formation in these basins, and raises the possibility that management of water within the catchment could be a means to enhance carbon capture within natural and artificial hyperalkaline lakes.

The geomorphological distribution of subaqueous tufa columns within a hypersaline lake: Mono Lake, USA.

C.E. Keevil, M. Rogerson*, D.R. Parsons, R. Mercedes-Martín, A.T. Brasier, J.J.G. Reijmer and A. Matthews

* Corresponding Author

Abstract

Understanding the flow of carbon through hyperalkaline lakes is a key means of understanding their biogeochemistry, sedimentology and their palaeoenvironmental and palaeoclimatic records. Furthermore, understanding how mineral precipitation is regulated in these lakes can provide insights into how their carbon sequestration behaviour can be managed. We report geophysical surveys of Mono Lake, California, USA, which show unanticipated geomorphological control on the recent / contemporary formation of lacustrine carbonate formations ("tufa"). Acquired shallow penetration seismic data shows a fault zone below the lake floor, but despite the regional evidence for geothermal waters rising up these fractures, we find no evidence for tufa precipitation at the surface exposure of this structure, either in the seismic data or in the swath bathymetry. However, we do find sub-lacustrine tufa columns in this data elsewhere, which is the first time these have been reported directly. We find and report on a strong link between column location and meteoric Ca supply to the lake, with the latter sourced either through surface runoff or groundwater. For example, a region close to a creek inlet has more frequent and larger tufa bodies, which grow at a wider depth range, than another region far from an inlet but close to the fault. This demonstrates the importance of meteoric water ingress in regulating carbonate mineral formation in these basins, and raises the possibility that

25 management of water within the catchment could be a means to enhance carbon
26 capture within natural and artificial hyperalkaline lakes.

27 **Introduction**

28 Saline and alkaline lakes are characteristic of volcanic landscapes today, forming
29 important habitats for wildlife, and hosting important communities of extremophile
30 microbes (Galat et al. 1990; Grant and Jones 2000; Jones et al. 1998; Melack 1981).
31 Carbonate minerals precipitated in these lakes can archive palaeoenvironmental data
32 (Kwiecien et al. 2014), entomb microfossils (Brasier et al. 2018) and macrofossils
33 (Smithson et al. 1993), and allow entrapment of significant volumes of organic carbon
34 (Saller et al. 2016). Research efforts recently have focused heavily on the flux of carbon
35 through alkaline geo-systems, and the potential for alkaline igneous terranes to
36 become sites of carbon capture and storage (Snæbjörnsdóttir et al. 2018).
37 Hyperalkaline lake waters and associated groundwaters are generally saturated with
38 respect to carbonate minerals (Rogers and Dreiss 1995a), and mineral precipitation is
39 limited by the availability of suitable cations – typically, calcium (Nielsen and DePaolo
40 2013). The carbon budget of these systems has been a point of investigation for
41 decades, and previous evaluations have generally emphasised the importance of
42 volcanic sources of both carbon and calcium (Oxburgh et al. 1991; Stine 1991).
43 However, the geomorphological controls on carbon supply to hyperalkaline
44 continental systems, and the control they place on the location and geometry of the
45 carbonate precipitate accumulations within them, have been less studied (Chavagnac
46 et al. 2013). Perhaps more significantly, geomorphological controls on the source of
47 calcium remain uncertain. Here, we seek to understand controls on the availability of
48 the limiting resource (calcium) to sites of carbonate precipitation in hyperalkaline
49 lakes (Nielsen and DePaolo 2013).

Mono Lake (California, USA: Fig. 1a) is an excellent example of a hyperalkaline system. It is a hydrographically closed hypersaline lake located in the Sierra Nevada, California (Brasier et al. 2018; Dunn 1953; Russell 1889; Stine 1990). Regional climate is classified as Mediterranean in the Köppen classification, with average winter temperature -6 ^{o}C and summer temperature 29 ^{o}C. Average minimum precipitation occurs as rain in September (0.3 mm day^{-1}) and maximum precipitation occurs as snow in February (0.26 cm day^{-1}). The lake lies within an area which is both tectonically and volcanically active (Colman et al. 2014), and has been extensively studied for its world-class volcanology (Cox et al. 2012), carbonate sedimentology (Benson 1981; Bischoff et al. 1993b; Newton 1994a), microbiology (Humayoun et al. 2003; Jellison and Melack 1993), ecology (Melack et al. 2017), geomagnetic history (Liddicoat and Coe 1979) and for its internal carbon budget (Oxburgh et al. 1991). Lake level has been very variable, providing key insights into past changes in the regional hydroclimate (Stine 1990; Zimmerman et al. 2006). Although there have been fluctuations in lake size and depth throughout the Holocene, the lake is not thought to have fully desiccated since its formation (Raumann et al. 2002; Scholl et al. 1967; Stine 1990). Shoreline deposits, especially the iconic tufa deposits (Scholl and Taft 1964; Selleck et al. 2007) show a very dynamic history, and water depth has varied by at least 40 m during the late Pleistocene, with highstands corresponding to North Atlantic cold phases (Benson and Thompson 1987; Wang et al. 2014). At present, the lake is at the lower end of its Pleistocene range, largely due to the diversion of feeder streams (Stine 1990). Water is primarily sourced from drainage of the Sierra Nevada in several creeks which provide ~2.21 x 10^{8} m^{3} water per year to the lake (Jones & Stokes 1993), along with a series of local groundwater and artesian thermal springs that are estimated to contribute < 15 % of inflow (Tomascak et al. 2003). The carbonate system of the lake is limited by low supply of calcium and compatible divalent metal ions (Nielsen and

DePaolo 2013), which is provided both by runoff water and through thermal spring water input (Clark and Hudson 2001). Steady state simulations suggest that hypersaline lake waters and fresher runoff groundwaters are dynamically connected precluding formation of an isolated pool of saline waters in the bottom of the lake (Rogers and Dreiss 1995a). Mono Lake is exceptionally placed as a laboratory in which to test the relative importance of the interaction between the subsurface saline (geothermal and lake water) and surface fresher (meteoric) sources of calcium in controlling carbonate mineral formation.

The sediments deposited within the lake basin are primarily comprised of: bio-siliceous material (primarily diatomaceous), carbonate components, and clay and carbonate debris (Newton 1994b). Although the carbonate has been considered to have had an abiogenic origin (Stine 1990; Zimmerman et al. 2006), more recent investigation has emphasized the role of cyanobacteria in controlling morphology, fabric and triggering of precipitation at least in the photic zone (Brasier et al. 2018). Carbonates from the most recent phase of rapid tufa formation, the early Holocene (Stine 1990), are distributed in a narrow belt just above the current lake level, exposed by the fall during the Anthropocene (Stine 1991). This Holocene phase of formation has been the focus of the majority of investigations, which emphasize the role of springs (Bischoff et al. 1993a; Shearman et al. 1989) in providing conditions for carbonate mineral growth. The carbonate deposits of the Mono basin include indurated sediment known locally as “sand tufa”, plus encrustations of shoreline country rock (largely dark coloured, porous tuffs), and woody vegetation, as well as the infamous “tufa columns” (Della Porta 2015; Scholl and Taft 1964; Souza-Egipsy et al. 2005). These are 1 m to 8 m tall, steep-sided carbonate bodies that developed subaqueously. The finding that cyanobacteria may have controlled growth of older

Pleistocene chimney structures (Brasier et al. 2018) implies chimneys originate within the photic zone, rather than tufa growth being driven solely by geothermal fluid flow along factures and through bedrock regardless of depth.

Mono Lake lies within a basin which remains volcanically active, with local volcanism dated to 0.3 Ma (Bailey and Hill 1990). The islands within the lake are evidence of recent magma replenishment, dating to the last 800 years (Stine 1990; Stine 2011); Negit Island (Fig 1b) represents the most northerly extent of this recent volcanism, with a rhyolite flow mapped to the north east of the island (Bursik and Sieh 1989). The largest island within the lake, Paoha Island, is also of volcanic origin – the northern third comprises the direct products of volcanism, with uplifted Pleistocene lake sediments forming the rest of the island (Lajoie 1968).

Colman *et al.* (2014) investigated the subsurface stratigraphy of the lake using seismic reflection data, concentrating in the western region with more limited investigation in the east. They identified 4 units of interest: i) an upper unit probably representing Holocene sedimentation; ii) a series of interbedded tephra's and interrupted lake sediments, which is thickest in the deep basin and thins to the basin edge; iii) a unit which is 12 m thick near Paoha Island but thins to 0.5 m within a few km; iv) finely-laminated lake sediments up to 1 m thick. Basal deposits within the lake basin date to ~67 ka BP according to radiometric and geomagnetic analysis (Zimmerman et al. 2006).

Here we explore two competing hypotheses concerning where encrusting carbonate production, and especially column formation, occur: i) they form wherever faults pierce the lake bed or ii) they develop in places confined to the shorelines, and reflect runoff. This connects with the more generic question regarding the role calcium

availability plays in controlling carbonate mineral formation in this type of geomorphic system. This paper aims to resolve these linked questions, using swath bathymetry and shallow penetration seismic data.

Previous Surveys of the Mono Lake floor

Using 3000 acoustic soundings Scholl *et al.* (1967) created a bathymetry map with a contour of 10 ft. A higher resolution survey was carried out by the Pelagos Corporation in 1986-1987, which has been summarized in a USGS DEM (Raumann et al. 2002). Depth data were collected at 15 m intervals (with an accuracy of +/-0.15 m) along a 1020 km survey lane, resulting in 29650 data points (Raumann et al. 2002); this survey did not correct for boat roll and pitch motion. As a result, these bathymetric data are too coarse to investigate the distribution of any tufa columns of dimensions similar to those observed on the lake shores within the lake itself. Raumann *et al.* (2002) were nonetheless able to identify the presence of several relict shorelines within the lake, most notably the so-called Scholl Terrace, which occurs at 1940.9 m (3.45 m below the lake surface in the present study). This terrace can be clearly observed within the USGS DEM of the lake (Raumann et al. 2002) and is thought to result from a significantly low lake level at ~1807 years BP (Stine 1990).

Methods

Fieldwork was carried out at Mono Lake from the 8th to the 10th October 2014, when the lake level was 1944.35 m (http://www.monobasinresearch.org/data/levelmonthly.php): we report all bathymetric and seismic data referenced to this level. Measurements were made of the lake bathymetry using a RESON 7125 Multibeam EchoSounder (MBES), sub-bottom structure using shallow seismic Innomar SES2000 profiler and of the lake water using

149 a Conductivity-Temperature-Depth probe (Valeport CTD). Two main study sites were
150 investigated: Area 1 in the westernmost basin of the lake, close to Lee Vining Creek
151 (western region); and, Area 2 to the east of Negit Island in the north of the lake (Fig.
152 1b). These sites were selected in order to provide two areas of contrasting
153 geomorphology, but are both adjacent to major developments of Holocene tufa
154 columns. Area 1 is a region of relatively low relief, implying that active faults along
155 which subsurface fluids may rise to form sub-lacustrine springs are unlikely to be
156 present. However, it is proximal to Lee Vining Creek, one of the most significant
157 sources of water from runoff and this is a key source of calcium to the lake system.
158 Area 2 is far from any surface flow, but within the steep topography related to the
159 islands within an area likely to contain faults. This maximizes the possibility of sub-
160 lacustrine springs, and a major spring is indeed known from Paoha Island (Williams
161 1997). Consequently, the selection of two regions permits us to interrogate parts of the
162 lake floor expected to exhibit the most recent carbonate encrustation development.

163 A high resolution Multibeam EchoSounder (MBES) survey of these areas was
164 undertaken with the system mounted on a small survey boat. This is a 400 kHz system
165 with an array of 512 formed beams operating in a swath angle of up to 128°, giving a
166 continuous track of depth measurements. A total of 38 km of MBES survey was
167 acquired across the two areas. A Leica 1230 differential Global Positioning System
168 (dGPS) with a real-time kinematic (RTK) correction was used to ensure accurate
169 spatial positioning to 0.02 m, with full real-time motion and heading correction
170 applied using an Applanix PosMV integrated motion-gyro system. Survey data were
171 collected using Hypack 2013 and processing of the bathymetry data was carried out
172 using Caris HIPS and SIPS version 7.1.2. Sound velocity corrections were made using
173 the data collected by the CTD system (see below). Surveying hypersaline waters causes

174 acoustic attenuation and is notoriously challenging. However, reducing the across-
175 track swath width through beam steering and running with very high system time-
176 varying gain settings, it was possible to detect and thus survey the lake bed.
177 Nonetheless, the high gain resulted in water column noise and some artefacts within
178 the data. In many areas these artefacts could be filtered and removed, but in some
179 areas, this has resulted in regions of missing data. Following processing within Caris
180 HIPS and SIPS the data were exported as a point cloud file at a resolution of (0.5 m)
181 to be analysed within ArcGIS. To measure the dimensions of lake floor objects,
182 including tufa columns, transects N/S and E/W were created across regions of interest
183 and measured using the profiling tool. Twenty representative columns were selected
184 for each area. To measure the dimensions of lake floor objects, including tufa columns,
185 intersecting NS and EW transects were created across objects of interest and measured
186 using the profiling tool in ArcGIS. Objects measured were selected based upon the
187 local quality of the multibeam data, to ensure that there were no artefacts from data
188 collection or holes in the interpolated surface, and where there was a single peak in the
189 data. The maximum depth at base, height of the object and width of the object was
190 calculated for each transect. The maximum value of these for each transect pair was
191 then selected for the object, and the final size of the object is the average of the two
192 measurements. In Area 1 the measurements of 72 objects are presented - 18% of the
193 total observed in the bathymetry data, making the result significant at 89% confidence
194 using Slovens formula (Altares et al. 2003). The objects were selected as representative
195 of the objects observed across the entire measurement area. The measurements of 27
196 objects in Area 2 are presented herein representing 14% of the observed objects
197 (significant at 82% confidence), representing all of the objects where an accurate size
198 could be measured. Most objects in Area 2 are very small / narrow, and the resolution
199 of the point cloud prevented accurate profiling. These objects generally had a

200 bathymetry difference of approximately 20 cm from the underlying surface, and so
201 were very small compared to columns known from the lake margin. This bias to large
202 objects will lead to an over-estimate of the size and abundance of carbonate objects
203 precipitating in this area.

204 In addition to the MBES bathymetric survey, approximately 20 km of shallow seismic
205 survey lines were collected, overlapping across the areas covered through the
206 bathymetric surveys described above. SonarWiz was used to post-process the data and
207 implement time corrections. Again, the dGPS RTK system was used for positioning
208 and motion (roll) was provided by the Applanix POS MV. Six transects were made in
209 Area 1 (Fig. 1c) and four in Area 2 (Fig. 1d). Three longitudinally north/south seismic
210 lines were also measured in Area 2 along with a longer transect which crossed these N
211 / S lines multiple times. The longest seismic section obtained, Line2-009, is 7.5 km in
212 length, crossing Area 2 from north to south, with 29 inflections (Fig. 1d).

213 The CTD-SVP measurements were mainly located in the northern region of the lake,
214 at the southern end of the main bathymetry measurements, with an additional pair of
215 data points to the west of Paoha Island and one within the western bathymetry section
216 (see Fig. 1d). Where a cast contained data for both instrument downcast and upcast,
217 following best practice only the downcast data are reported here. Pressure data were
218 converted to depths using the Valeport DatalogX2 Sea Water Calculation wizard
219 (Valeport, 2008 & 2015; http://www.valeport.co.uk/Support/Software). The Chen
220 and Millero (1977) Speed of Sound Formula was used for the conversion (Chen and
221 Millero 1977).

222 Major ion composition of Mono Lake waters and representative inflowing waters were
223 provided from samples taken during October 2014. A filtered (0.45 μm) water sample

224 was taken and acidified immediately with HNO_3 in preparation for trace metal
225 analysis by a Perkin Elmer Optima 5300DV inductively coupled plasma optical
226 emission spectrometer (ICP-OES) at the University of Hull. A blank and standard suite
227 were analysed every 15 samples to check instrument calibration, and wavelengths were
228 selected in accordance with standard methods (USEPA Method 200.7).

229 **Results**

230 **Bathymetry**

231 The smaller of the two study sections, Area 1 (160 m wide and 800 m long; Fig. 1c),
232 has good multibeam coverage throughout (Fig. 2), with water depths between 2 m at
233 the southern edge to 16.5 m at the northern end of the section. The southern shoreline
234 of the section is rocky in nature, while the deeper sections are generally featureless.
235 Pinnacle-shaped constructions are observed throughout (Fig. 2), ranging in height
236 from 0.5 - 4.1 m, although most are approximately 1.0 m in height. The tallest of the
237 interpreted sub-lacustrine tufa columns measured is 4.15 m, with three other columns
238 measuring over 2 m (Figs. 2 and 9). These columns are found at random throughout
239 the section, with no clustering or organized distribution observed.

240 The larger bathymetry section, Area 2, was measured to the east of Negit Island in the
241 north of the lake (Fig. 1d). The section is 2500 m long and 400 m wide, adjacent to
242 several rocky islets (Fig. 3), ranging in depth from 1.5 m at the north of the section to
243 25 m in the south. Most of the bathymetry is featureless, with column-like objects only
244 observed in the shallow region (<2.5 m water depth) at the north of the section (Fig.
245 3a). The column-like objects range in height from 0.25 – 0.75 m within this sub-area.
246 At the south of the section, bathymetry measurements were made surrounding a small
247 volcanic islet, with irregular features found on the islet slopes. A break in slope with a

general east-west orientation marks the boundary between the shallower sediments to the north and the deeper basin in the south (Fig. 3b). Within the deeper basin some isolated structures are present, which are larger than the column-like objects observed at the north of Area 2, and with distinctive geometry. Indeed, these structures are much larger than columns observed elsewhere in the Mono Lake region, both in height and surface area. They are located at the edge of the bathymetry section, adjacent to a volcanic islet.

Seismic profiles

Seismic measurements were made across both bathymetry sections, both longitudinally and across the sections, allowing the relationship of surface and subsurface to be inferred (Figs. 4 and 5). The transects in Area 1 show a clear surface, with a strong echo at ~ 20 ms below this main surface: any surface structures correspond to the previously described bathymetry, although there is no subsurface expression. A subsurface layer is observed in all lines above the strong multiple, which shows some rounded structures, occasionally corresponding to surface structures visible in the bathymetry data adjacent to the seismic transect (Figure 2).

A distinct surface is present in all seismic transects (Figs. 6 and 7), however there is no evidence of a deeper buried surface as observed in Area 1, although a strongly exaggerated multiple is present. Buried features are observed within all transects, often expressed with a second echo. Line-007 is 2.1 km long and measures down the centre of Area 2 moving north-south (Fig. 6). At the southern end are clear columns at 15 ms which are also visible in the bathymetric surface. There is evidence of sedimentation overlying a slightly older surface at several places in the section (Figs. 6 and 7, highlighted in red). These draped sediments have a strong reflector with a

continuous trace, and correspond to relatively featureless areas within the bathymetry surface. An exaggerated multiple is observed which repeats this underlying surface. There is no draping sediment observed adjacent to the southern columns.

Line2-007 is 2 km long, originating at the south of Area 2 and moving northwest for the first 170 m before moving north along the western edge of the bathymetry measurements (Fig. 7a). The first 2000 traces measure the edge of a small island, which rises 15 ms from the bed. Within the north-south region of the seismic line the bed is relatively featureless, with small rises at traces 3000, 4500 and 8500. These correspond to featureless highs within the bathymetry data. However, an older horizon is visible <5 ms below the present surface, which is repeated in the strong bed multiple within the data. As in Line-005 and Line-006 in Area 1 the inclination of reflectors into deeper basins appear to show reworking of sediment off narrow highs. The reworked high at trace 8500 shows a lack of subsurface data similar to those observed in the previous lines, and it may be a fallen column. It corresponds to an unclear local high within the bathymetry data, but does not lie within the region of columns observed at the north of Area 2.

Line2-008 (Fig. 6c) is 950 m long, located at the east of the section and was measured in a south-north orientation. The bed surface is relatively featureless, as shown in the bathymetry, with no internal structure for the majority of its length. At the northern part of the line a local high is observed, which is also clearly visible in the bathymetry data. The seismic line shows that this high has two steeply dipping planes oriented to the south. A strongly dipping horizon is also visible in Line2-007 at trace 3000, which corresponds to the edge of the same high in the west. However, in Line2-007 this edge has been reworked and draped with sediments, so it is unclear if it is the same feature.

296 The first 8 sub-sections of Line2-009 (Fig. 7, <trace 9000), measure the rather
297 featureless high observed at the north of the bathymetry section. Buried structures are
298 present at traces ~1250 and 6000, with draped overlaying sediments, which is
299 repeated in the surface multiple. The structure between Inflection 5 (trace 5100) and
300 Inflection 6 (trace 6750) corresponds to the same high observed in Line2-007 (Fig. 6a,
301 trace 8500), and shows the same surrounding draped sediments. The buried surface
302 present at Inflection 8 (Fig. 7) possibly represents the lateral extension of this feature
303 to the southwest. Steeply dipping surfaces adjacent to Inflection 9 (outside bathymetry
304 surface), after Inflection 13 and before Inflection 15 appear to be the same structures
305 observed in Line2-008 (Fig. 6c). The dipping surface present in Line2-008 (Fig. 6c)
306 corresponds to ~ trace 27500, just before Inflection 17 in Line2-009 (Fig. 7), which
307 does not appear to extend below the surface in this line, due to the different angle and
308 subsurface noise, although it is visible in the data at Inflection 20 (Fig. 7). The apparent
309 peak at Inflection 18 (Fig. 7) is due to a local topographic high, although this does
310 appear to result from sedimentation overlying an older structure, and there is no
311 indication of this structure in the subsurface. This is also the case at Inflection 22 (Fig.
312 7) (adjacent to the island as in Line2-007, Fig. 6a), Inflections 24, 26 and 28
313 correspond to columns at the south Area 2 (Fig. 7).

314 **Water column structure**

315 Sound velocity, temperature and conductivity data were obtained from CTD casts
316 located within both measurement regions, as well as to the west of Negit Island (Fig.
317 1b and Figure 8). These values fall into two distinct groups: the data collected within
318 Area 2 (Casts 5, 13, 15, 20 and 22); data collected to the west of Paoha Island (Area 1:
319 Cast 30; Island region: Casts 24 and 25). The temperatures measured in Area 2 are
320 higher, with correspondingly higher sound velocity and conductivity values. All

samples within the bathymetry sections were collected at a water depth of less than 13 m, with little variation in temperature and conductivity values with depth. The two casts made in deeper water (Casts 24 and 25) reveal a stratification surface at a depth of 13 m.

Discussion

Lake Stratification

Comparison of conductivity and temperature data from the CTD-SVP casts reveal that they agree with values previously obtained from formerly reported brine samples by Jellison *et al.* (1999), although there are some outliers in the deepest values (Figure 8). There is a distinct region of stratification observed in the samples obtained west of Paoha Island (Fig. 1b) at a depth of ~13 m which is likely to correspond to both the pycnocline (MacIntyre et al. 1999) and thermocline (Vidal et al. 2013) observed in earlier surveys at similar depths. A similar chemocline at 15m is reported from 2017 (Phillips et al. 2021). Mono Lake alternates between being meromictic and monomictic depending on the quantity of freshwater introduced during snowmelt from Sierra Nevada and the proportion diverted to the City of Los Angeles (Melack et al. 2017). A transition to meromictic stages occurred in 1984 and in 1994-5 (Davis 1999; Melack and Jellison 1998; Melack et al. 2017), and repeated observation of a robust chemocline from 1994 to 2017 at approximately the same depth (13 m – 15 m) demonstrates this is now the established structure of the water column. Jellison *et al.* (1998) predicted that stratification may continue for several decades as the water level increases due to changes in local management practices, and this prediction is fully confirmed by these findings.

There is variation in the depth of the chemocline observed between the measurements made to the east and west of Paoha Island, with higher temperature, conductivity and sound velocity values observed within Area 1 similar to that described ~10 years earlier (Vidal et al. 2013) suggesting continuity of stratification (Fig. 8). Such thermal fluctuations in the surface lake have been previously attributed to variations on the internal waves' dynamics associated to wind intensities and associated seiche, the layered density structure of the lake, and basin morphometrics (Vidal et al. 2013).

Lake bottom characteristics

Bathymetry measurements in both Area 1 to the west of the lake and Area 2 to the northeast of the lake revealed the presence of interpreted submerged tufa columns (Figs 1, 2 and 3). In Area 2, columns were only observed at October 2014 water depths of less than 2.5 m, but no relationship with water depth was found in Area 1. Area 1 varied in depth from 2 m (minimum measurable depth for our system) adjacent to the southern shoreline to 16.5 m at the north of the area. In addition, subaerial columns interpretable as tufa were observed throughout this area, with no clustering or linear organization, suggesting their independence from any spring point or line, or from flow from a fracture.

In addition to the columns observed in the bathymetry measurements, shallow seismic data were collected to examine the presence of any columns associated with buried lake sediments. Previous seismic studies of Mono Lake (Colman et al. 2014) have revealed four distinct seismic-stratigraphic units. Whilst columns are observed on the surface of Area 1 there is no clear evidence for any in the subsurface (Figs. 4, 5, 6 and 7). An older surface is visible, but any structures present have been heavily eroded. This featureless sub-surface is suggestive of the uppermost unit observed by Colman

368 *et al.* (2014), which they characterize as containing weak but continuous internal
369 reflections. This unit is not observed throughout their measurements, but was seen in
370 a line measured to the northeast of Area 1. The subsurface of Area 2 shows eroded
371 columns further south than those visible in the bathymetry data (Figs 6 and 7); these
372 have been eroded and the surface topography infilled by sediment, which although
373 presenting a strong seismic reflection at the surface does not create a multiple.
374 Strongly dipping surfaces adjacent to topographic highs visible in Area 2 appear to
375 show local uplift, with adjacent sediment infill. The large, steep-sided objects noted in
376 this region in Results (above) observed at the south of Area 2 do not have subsurface
377 structures and are larger than known tufa (Della Porta 2015; Stine 1990) columns.
378 They show adjacent sediment infill, suggesting that they have formed relatively
379 recently (Fig. 6c), and are probably gravity flow debris from the adjacent island.

380 **Tufa Columns**

381 We present here the highest resolution bathymetry data recorded to date within Mono
382 Lake. The new data represent less than 1% of the lake bed, however there is a
383 considerable improvement in the quality and resolution compared to lake-wide survey
384 data (Raumann et al. 2002). This new dataset reveals a localised distribution of tufa
385 columns (Figs. 2 and 3), with differences between two surveyed areas apparently
386 arising from their different geomorphological setting. As with the Great Salt Lake
387 (Utah, USA) and other saline lakes from the wider region, we find carbonate
388 development is restricted to the shallow water parts of the lake (Bouton et al. 2016;
389 Colman et al. 2002), consistent with a strong water depth control on formation
390 (Bouton et al. 2016). The new data are sufficiently highly resolved to determine the
391 geometry of these sub-lacustrine columns (Fig. 9). Comparison of column heights and
392 widths with depth show that the two locations have very different geometries (Fig. 9).

393 The shallow-water columns in Area 2 are both shorter and narrower than all the
394 columns observed within Area 1, despite the selection of relatively large objects from
395 Area 2 tending to bias the analysis in the opposite sense. There is considerably less
396 volume of carbonate present in Area 2 compared to Area 1, reflecting markedly lower
397 production of carbonate. This is likely reflecting an enhanced discharge from Sierra
398 Nevada freshwater sources in Area 1 compared to those from the north-eastern
399 shoreline close to the volcanogenic islands (Rogers and Dreiss 1995a) (see creek fluxes
400 and catchment areas in Fig. 1b).

401 The strongly dipping feature observed at a water depth of ~ 10 m within both the
402 bathymetry data and seismic data presented here (Figs. 3 and 7) further supports this
403 interpretation. Although it lies to the west of a previously suggested position (Bailey
404 1989), this is a significant sub-lacustrine fault. Previous analysis of subaerial tufa
405 columns within the wider Mono Basin has shown that they form adjacent to local
406 faults, with formation associated with springs (Brasier et al. 2018). However, we can
407 find no indication of potential carbonate growths along this fault at either the lake floor
408 or in the subsurface. This must indicate: i) there is no groundwater exiting across this
409 fault to the lake waterbody, ii) water is circulating throughout sub-bottom faults but
410 calcium supplied through this route is not effective in constructing tufa encrustations,
411 or iii) these faults are conduits for advective transport of solutes from the lake to
412 groundwater by density-driven convection (Rogers and Dreiss 1995b).

413 Studies of the local groundwater reveal that at higher lake stages, the shoreline
414 freshwater discharge zone moves toward the basin edge, and the unrestrained saline
415 lake groundwater mass subsides, drawing solutes from the lake down into the basin
416 sediments (Rogers and Dreiss 1995b). These processes could explain the lack of Ca-
417 rich groundwater fluxes into the lake at specific depths where the high saline and dense

418 lake waters tend to infiltrate as occurs in many evaporative basins (Wood and Sanford
419 1990). This eliminates the possibility of tufa column construction at sites of lake water
420 seepage towards groundwater aquifers.

421 The simplest explanation for the occurrence of sub-lacustrine columns is therefore
422 that carbonate minerals are precipitated wherever invading waters first contact the
423 highly alkaline lake water. The lake water is saturated with respect to both calcite and
424 aragonite (Rogers and Dreiss 1995b) and precipitation is already highly favoured
425 thermodynamically (Rogerson et al. 2014). The lack of actively forming precipitation
426 is consequently the limiting availability of calcium, which in lake waters is between 3-
427 3.4 mg L^{-1} (Table 1). This likely poses a kinetic limitation on the rate of precipitation,
428 as where the ratio of Ca : CO_3 deviates significantly from unity crystal assembly is
429 impeded (Wolthers et al. 2012). Generally higher Ca availability in runoff water (6.7-
430 8.5 mg L^{-1}) and in cool (2.2 - 111.9 mg L^{-1}) and warm (17 – 32 mg L^{-1}) springs provides
431 feedstock for $CaCO_3$ formation, and accelerates its growth by moving the Ca : CO_3 ratio
432 towards unity. Consequently, enhanced growth in the mixing zone will likely be
433 strongly favoured in this system. The most favourable window for tufa formation is
434 thus located between the lake shoreline and the depth of the interface between fresher
435 groundwater and where alkaline and hypersaline lake waters infiltrate the
436 groundwater (Rogers and Dreiss 1995a). The position of this interface will depend on
437 several factors such as the water table hydrological conditions, permeability of lake
438 bottom sediments, wind intensities, and the evolving position of lake level (Rogers and
439 Dreiss 1995a; Rogers and Dreiss 1995b; Vidal et al. 2013).

440 The thin and short columns in the shallowest parts of Area 2 (Fig. 3) reflect the weak
441 advection of groundwater into the lake, and the much higher carbonate production
442 and extensive distribution of columns in Area 1 reflect calcium supply via Lee Vining

443 Creek and associated groundwater. Provision of calcium via meteoric groundwater in
444 Area 1 is consistent with direct observation of groundwater chemistry. Although much
445 of the groundwater below Mono Lake is saline, essentially being lake water, which has
446 infiltrated the subsurface, there is a rim of relatively fresh groundwater which follows
447 the shore of the lake to the north and east, where Area 1 is positioned. Towards the
448 western edge of Mono Lake, groundwater becomes less saline due to run-off from the
449 Sierra Nevada (Rogers and Dreiss 1995a), and this freshwater intrusion extends as far
450 as Paoha Island, thus occupying the entire space below Area 1, consistent with the
451 higher production of carbonate in this sector. Consequently, although the carbon in
452 solution is largely considered to be geothermal in origin on the basis of its radio-
453 isotope characteristics (Oxburgh et al. 1991), it is precipitated by titration against
454 cations provided from the meteoric realm, largely supplied via surface flow.

455 High-resolution microscopy has previously revealed well-preserved microbial fossils
456 within Mono Lake tufa tower carbonate (Brasier et al. 2018). These deposits were fossil
457 (Pleistocene) and calcitic rather than aragonitic so differences in nucleation pathways
458 cannot be ruled out when comparing nucleation processes between these columns and
459 those in the lake in recent times, especially in terms of lake productivity and water
460 turbidity. However, it is likely the distribution and style of carbonate precipitation we
461 observe will have some microbiological overprint. Surface waters in Mono Lake today
462 are highly productive, with algal and cyanobacterial communities both producing high
463 concentration of particulate organic matter (up to 1.5 mM L^{-1}) and chlorophyll a (up to
464 100 μg L^{-1}) (Phillips et al. 2021). This high productivity produces high water turbidity
465 and photosynthetically active radiation falls rapidly with depth, and no detectable light
466 can be found below 15m (Phillips et al. 2021). On that basis, microbiological evaluation
467 of the lake suggests that there is little of the observed chlorophyll a being produced by

468 benthic photosynthesis (Phillips et al. 2021), and this material on the sediment surface
469 was produced in surface water. Degradation of the abundant organic matter observed
470 settling through the water column, or chemosynthetic activity within the dysoxic
471 bottom waters of the lake remain likely microbiological mechanisms for altering and
472 enhancing mineral nucleation. Equally, degradation of organic matter in the deep
473 basin may suppress nucleation by consuming alkalinity within sediment pore waters.
474 Further investigation will be needed to evaluate these processes, but from the available
475 data neither seem sufficient to overprint the impact of calcium source location to
476 determine the spatial distribution of sublacustrine tufa build-ups.

477 The dominance of surface flow in controlling where tufa columns form spatially
478 implies a similar seasonality control. Discharge from the creeks providing water and
479 calcium to the lake (Fig 1b) is highly seasonal (Fig. 10), with generally low discharge
480 (<1 $m^3 s^{-1}$) occurring outside the period of snowmelt in the spring and early summer
481 (April-August). As peak discharge occurs in June we also expect to find peak tufa
482 production at that time, or following a short lag. Testing this hypothesis and
483 characterising the length of the time lag are stimulating questions for future research.

484 Given the role of microbial biofilms in promoting the formation of tufa chimneys
485 previously reported (Brasier et al. 2018), it is likely both location and timing of
486 carbonate precipitation is complicated by either photosynthesis, or organic
487 degradation or both. We were unable to recover samples of actively-forming tufa from
488 the sublacustrine part of the lake, which limits our ability to determine the nature and
489 degree of this influence. However, photosynthesis is thought to be restricted to the
490 upper parts of the water column due to high turbidity leading to rapid light attenuation
491 with depth (Phillips et al. 2021), so chemosynthetic metabolisms or release of chelated
492 ions during organic matter degradation are more likely mechanisms. Consumption of

alkalinity in the anoxic sediment pore water may also lead to suppression of precipitation, but there is no evidence of accumulation of calcium and magnesium in sub-chemocline water which would suggest this extends into the water column (Phillips et al. 2021). Biological processes therefore likely play a secondary role in determining the location and timing of carbonate mineral formation.

Wider significance

Despite the dominance of the carbon budget of hyperalkaline lakes by geothermal input (Oxburgh et al. 1991), precipitation and sequestration of this carbon is regulated by hydrological fluxes and the dynamic behaviour of the fresh-hypersaline groundwater interface, and is ultimately controlled by the solute mass balance between waters entering and exiting the lake (Sanford and Wood 1991). This may influence productivity of carbonate within the lake in areas with heterogeneous calcium input, and also alter the precipitation mechanisms and the character of the precipitate in different areas. Moreover, this process also predicts that significant carbonate is being produced at specific lake depths. Ultimately, this complexity reflects that the system is calcium-limited, a feature held in common with subaerial travertine systems. The overall behaviour of the system is therefore dependent on the availability of these cations, and almost independent of the availability of carbon, which is ubiquitous. A schematic model for the precipitation we observe is provided in Figure 11.

The prediction of significant sub-lake carbonate precipitation has profound implications for understanding alkaline lake sedimentology which will need to distinguish between deposits formed in hydrologically closed basins and those accumulated in open lake basins (Dutkiewicz et al. 2000; Mercedes-Martín et al.

517 2019). Equally, considering whether carbonate has formed within the lake water or
518 below sediment surface within infiltrating waters may alter interpretation of
519 palaeoenvironment signals from lake cores and palaeo-lake sequences (Kwiecien et al.
520 2014). Likewise, for paleoclimate studies this diagenetic carbonate is not being
521 produced within the lake itself and is unlikely to be in equilibrium with surface climate.
522 Finally, this may open further avenues for investigation of carbonate formation on the
523 early Earth and on other planets motivated by the search for microbial signatures (e.g.
524 Gale Crater, Jezero Crater and Oxia Planum on Mars (Horgan et al. 2020; Sutter et al.
525 2017), as sub-lake floor environments and deposits will need to be investigated if
526 calcium ions are not passing into open-lake environments.

527 The control of carbon sequestration within these lakes by meteoric calcium implies
528 that managing the water flow into them, and the land management in their catchment,
529 will alter the rate of carbon fixation. This places hyperalkaline lakes within the sphere
530 of environments in which passive carbon management can be achieved by good
531 environmental stewardship, and without energy-intensive practices such as injection
532 of gasses into igneous bedrocks (Snæbjörnsdóttir et al. 2018). Today, the Los Angeles
533 Department of Water & Power are permitted to divert up to 16,000 acre-feet of runoff
534 from the lake to other uses. Permitting this water to enter the lake would likely result
535 in ~500 tonnes of calcite precipitation per year, which will aggregate in other
536 catchments through the region where water is being diverted from endorheic lakes.
537 There is therefore an opportunity within systems like Mono Lake both for improved
538 management of naturally occurring hyperalkaline water bodies but also for
539 construction and management of artificial reservoir facilities in regions with suitable
540 rocks which are weathering at the surface within a wider catchment.

541 **Conclusions**

Although additional bathymetry mapping is required to fully quantify the locations of tufa columns within the lake, we show that although sub-lacustrine tufa columns do occur within Mono Lake (California, USA), they are not equally nor randomly distributed. They also do not cluster or align within subsurface tectonic features, which would be expected to control geothermal water ingress. Rather, the most frequent, largest and deeper-water tufa growth is occurring within areas affected by groundwater and runoff water entering the lake from the meteoric realm, with relatively high calcium content. The lower limit of this tufa-formation zone is the interface between this relatively low-density water and more saline lake-interior water, and is thus largely dependent on local hydrological oscillations, lake bottom sediment permeability, wind intensities, and the relative variations of the lake level.

At depths below the influence of meteoric water, advective infiltration of lake waters down to groundwater aquifers and lake sediments can seriously restrict tufa carbonate growth. Carbonate formation is therefore sectored in a manner which mimics water mass physico-chemical characteristics, and the deeper, denser and hypersaline part of the lake appears to not be a site of carbonate mineral precipitation.

Below the deep part of the lake, rising geothermal calcium is reacted with lacustrine groundwater to form carbonate bodies below the lake bottom, potentially complicating the paleolimnology archive of these deposits. Such significant and widespread early diagenetic carbonation suggests carbonate recovered in cores is not necessarily being produced within the lake itself, and may not be in equilibrium with the surface system.

Equally, the regulation of carbonate precipitation by runoff water raises the possibility of managing lake carbon sequestration performance via regulating calcium supply. Increased flow of water into the lake, or increased concentration of calcium within that

water are both achievable by appropriate catchment management. This may provide new means of carbon sinking within natural lakes, and artificially constructed reservoirs may also provide an additional means of sinking carbon within catchments with suitable geology.

Acknowledgments

This work was supported by funding from BP Group. We thank the Mono Lake Committee for supporting fieldwork and for helping our vessel onto and most of all off the lake, and the State of California for permitting access to the lake and its environs. Dave Marquart is thanked for his support and knowledge of the lake environment. Cody and Phillip are thanked for their help on the lake, and Vern for vital logistical support. Ian Billing is thanked for his instrumental involvement in this project, and his role in shaping our thoughts. We hope he would be pleased with this paper. Dr. Chelsea Pederson, Dr. W. Fischer are heartily thanked for their excellent efforts as reviewers improving this manuscript, and Dr. Juan Carlos Laya is thanked for his careful handling of the manuscript as Associate Editor.

References

Altares, P., Copo, A., Gabuyo, Y., Laddaran, A., Mejia, L., Policarpio, I., Sy, E., Tizon, H., and Yao, A., 2003, Elementary Statistics: A Modern Approach: Rex Bookstore Inc., Manila, Philippines.

Bailey, R.A., 1989, Geologic Map of Long Valley Caldera: Mono-Inyo craters volcanic chain, and vicinity, eastern California: US geological survey miscellaneous investigations map I-1933, scale, v. 1, p. 11.

Bailey, R.A., and Hill, D.P., 1990, Magmatic Unrest at Long Valley Caldera, California, 1980-1990: Geoscience Canada.

590 Benson, L.V., 1981, Paleoclimatic Significance of Lake-Level Fluctuations in the
591 Lahontan Basin. : Quaternary Research, v. 16, p. 390-403.
592 Benson, L.V., and Thompson, R.S., 1987, Lake-Level Variation in the Lahontan Basin
593 for the Past 50,000 Years: Quaternary Research, v. 28, p. 69-85.
594 Bischoff, J.L., Stine, S., Rosenbauer, R.J., Fitzpatrick, J.A., and Stafford Jr, T.W.,
595 1993a, Ikaite Precipitation by Mixing of Shoreline Springs and Lake Water,
596 Mono Lake, California, USA: Geochimica Et Cosmochimica Acta, v. 57, p. 3855-
597 3865.
598 Bischoff, J.L., Stine, S., Rosenbauer, R.J., Fitzpatrick, J.A., and Stafford, T.W., 1993b,
599 Ikaite Precipitation by Mixing of Shoreline Springs and Lake Water, Mono
600 Lake, California, USA: Geochimica et cosmochimica acta, v. 57, p. 3855-3865.
601 Bouton, A., Vennin, E., Boulle, J., Pace A., Bourillot R., Thomazo, C., Brayard, A.,
602 Désaubliaux, G., Goslar, T., Yokoyama, Y., and Dupraz, C., 2016, Linking the
603 Distribution of Microbial Deposits from the Great Salt Lake (Utah, USA) to
604 Tectonic and Climatic Processes.: Biogeosciences, v. 13.
605 Brasier, A., Wacey, D., Rogerson, M., Guagliardo, P., Saunders, M., Kellner, S.,
606 Mercedes- Martin, R., Prior, T., Taylor, C., Matthews, A., and Reijmer, J.J.G.,
607 2018, A Microbial Role in the Construction of Mono Lake Carbonate
608 Chimneys?: Geobiology, v. 16, p. 540-555.
609 Bursik, M., and Sieh, K., 1989, Range Front Faulting and Volcanism in the Mono
610 Basin, Eastern California. : Journal of Geophysical Research: Solid Eart, v. 94,
611 p. 15587-15609.
612 Chavagnac, V., Ceuleneer, G., Monnin, C., Lansac, B., Hoareau, G., and Boulart, C.,
613 2013, Mineralogical Assemblages Forming at Hyperalkaline Warm Springs
614 Hosted on Ultramafic Rocks: A Case Study of Oman and Ligurian Ophiolites:
615 Geochemistry, Geophysics, Geosystems, v. 14, p. 2474-2495.

616 Chen, C.T., and Millero, F.J., 1977, Speed of Sound in Seawater at High Pressures: The
617 Journal of the Acoustical Society of America, v. 62, p. 1129-1135.
618 Clark, J.F., and Hudson, G.B., 2001, Quantifying the Flux of Hydrothermal Fluids into
619 Mono Lake by Use of Helium Isotopes: Limnology and Oceanography, v. 46, p.
620 189-196.
621 Colman, S.M., Hemming, S.R., Stine, S., and Zimmerman, S.R.H., 2014, The Effects of
622 Recent Uplift and Volcanism on Deposition in Mono Lake, California, from
623 Seismic-Reflection (Chirp) Profiles: Journal of Geophysical Research B: Solid
624 Earth, v. 119, p. 3955-3970.
625 Colman, S.M., Kelts, K.R., and Dinter, D.A., 2002, Depositional History and
626 Neotectonics in Great Salt Lake, Utah, from High-Resolution Seismic
627 Stratigraphy:: Sedimentary Geology, v. 148, p. 61–78.
628 Cox, S.E., Farley, K.A., and Hemming, S.R., 2012, Insights into the Age of the Mono
629 Lake Excursion and Magmatic Crystal Residence Time from (U- Th)/He and
630 230 Th Dating of Volcanic Allanite: Earth and Planetary Science Letters, v. 319,
631 p. 178-184.
632 Davis, O.K., 1999, Pollen Analysis of a Late-Glacial and Holocene Sediment Core from
633 Mono Lake, Mono County, California: Quaternary Research, v. 52, p. 243-249.
634 Della Porta, G., 2015, Carbonate Build-Ups in Lacustrine, Hydrothermal and Fluvial
635 Settings: Comparing Depositional Geometry, Fabric Types and Geochemical
636 Signature: Geological Society, London, Special Publications, v. 418, p. 17-68.
637 Dunn, J.R., 1953, The Origin of the Deposits of Tufa in Mono Lake [California]:
638 Journal of Sedimentary Research, v. 23, p. 18-23.
639 Dutkiewicz, A., Herczeg, A., and Dighton, J., 2000, Past Changes to Isotopic and
640 Solute Balances in a Continental Playa: Clues from Stable Isotopes of Lacustrine
641 Carbonates: Chemical Geology, v. 165, p. 309-329.

642 Galat, D.L., Verdin, J.P., and Sims, L.L., 1990, Large-Scale Patterns of Nodularia
643 Spumigena Blooms in Pyramid Lake, Nevada, Determined from Landsat
644 Imagery : 1972-1986: Hydrobiologia,, v. 197, p. 147-164.
645 Grant, W.D., and Jones, B.E., 2000, Alkaline Environments, *in* Lederberg, J., ed.,
646 Encyclopedia of Microbiology, Academic Press.
647 Horgan, B.H., Anderson, R.B., Dromart, G., Amador, E.S., and Rice, M.S., 2020, The
648 Mineral Diversity of Jezero Crater: Evidence for Possible Lacustrine Carbonates
649 on Mars: Icarus, v. 339, p. 113526.
650 Humayoun, S.B., Bano, N., and Hollibaugh, J.T., 2003, Depth Distribution of
651 Microbial Diversity in Mono Lake, a Meromictic Soda Lake in California:
652 Applied and environmental microbiology, v. 69, p. 1030-1042.
653 Jellison, R., and Melack, J.M., 1993, Algal Photosynthetic Activity and Its Response to
654 Meromixis in Hypersaline Mono Lake, California. : Limnology and
655 Oceanography, , v. 38, p. 818-837.
656 Jones & Stokes, A., 1993, Environmental Impact Report for the Review of Mono Basin
657 Water Rights of the City of Los Angeles. Draft. : Sacramento, CA, Prepared for
658 California State Water Resources Control Board, Division of Water Rights, .
659 Jones, B.E., Grant, W.D., Duckworth, W., and Owenson, G.G., 1998, Microbial
660 Diversity of Soda Lakes.: Extremophiles, v. 2, p. 191-200.
661 Kwiecien, O., Stockhecke, M., Pickarski, N., Heumann, G., Litt, T., Sturm, M.,
662 Anselmetti, F., Kipfer, R., and Haug, G.H., 2014, Dynamics of the Last Four
663 Glacial Terminations Recorded in Lake Van, Turkey: Quaternary Science
664 Reviews, v. 104, p. 42-52.
665 Lajoie, K.R., 1968, Quaternary Stratigraphy and Geologic History of Mono Basin,
666 Eastern California, Unpublished Ph. D. Dissertation, University of California
667 Berkeley.

668 Liddicoat, J.C., and Coe, R.S., 1979, Mono Lake Geomagnetic Excursion: Journal of
669 Geophysical Research: Solid Earth, v. 84, p. 261-271.
670 Macintyre, S., Flynn, K.M., Jellison, R., and Romero, J.R., 1999, Boundary Mixing and
671 Nutrient Fluxes in Mono Lake, California: Limnology and Oceanography, v. 44,
672 p. 512-529.
673 Melack, J.M., 1981, Photosynthetic Activity of Phytoplankton in Tropical African Soda
674 Lakes: Hydrobiologia, v. 81, p. 71-85.
675 Melack, J.M., and Jellison, R., 1998, Limnological Conditions in Mono Lake:
676 Contrasting Monomixis and Meromixis in the 1990s: Hydrobiologia, v. 384, p.
677 21-39.
678 Melack, J.M., Jellison, R., Macintyre, S., and Hollibaugh, J.T., 2017, Mono Lake:
679 Plankton Dynamics over Three Decades of Meromixis or Monomixis., Ecology
680 of Meromictic Lakes, Springer, p. 325-351.
681 Mercedes-Martín, R., Ayora, C., Tritlla, J., and Sánchez-Román, M., 2019, The
682 Hydrochemical Evolution of Alkaline Volcanic Lakes: A Model to Understand
683 the South Atlantic Pre-Salt Mineral Assemblages: Earth-Science Reviews, v.
684 198, p. 102938.
685 Newton, M.S., 1994a, Holocene Fluctuations of Mono Lake, California: The
686 Sedimentary Record.: Sedimentology and Geochemistry of Modern and
687 Ancient Saine Lakes. SEPM Special Publication, v. 50.
688 Newton, M.S., 1994b, Holocene Fluctuations of Mono Lake, California: The
689 Sedimentary Record., *in* Renaut, R.W., and Last., W.M., eds., Sedimentology
690 and Geochemistry of Modern and Ancient Saline Lakes: Sepm Special
691 Publications, SEPM, p. 143-157.

692 Nielsen, L.C., and Depaolo, D.J., 2013, Ca Isotope Fractionation in a High-Alkalinity
693 Lake System: Mono Lake, California: Geochimica et Cosmochimica Acta, v. 118,
694 p. 276-294.
695 Oxburgh, R., Broecker, W.S., and Wanninkhof, R.H., 1991, The Carbon Budget of
696 Mono Lake: Global Biogeochemical Cycles, v. 5, p. 359-372.
697 Phillips, A.A., Speth, D.R., Miller, L.G., Wang, X.T., Wu, F., Medeiros, P.M.,
698 Monteverde, D.R., Osburn, M.R., Berelson, W.M., Betts, H.L., Wijker, R.S.,
699 Mullin, S.W., Johnson, H.A., Orphan, V.J., Fischer, W.W., Geobiology, C.,
700 Geobiology, C., and Sessions, A.L., 2021, Microbial Succession and Dynamics
701 in Meromictic Mono Lake, California: Geobiology, v. 19, p. 376-393.
702 Raumann, C.G., Stine, S., Evans, A., and Wilson, J., 2002, Digital Bathymetric Model
703 of Mono Lake, California: Miscellaneous field studies map MF-2393. US
704 Geological Survey, Menlo Park, CA. https://pubs. usgs. gov/mf/2002/2393.
705 Rogers, D.B., and Dreiss, S.J., 1995a, Saline Groundwater in Mono Basin, California:
706 1. Distribution: Water Resources Research, v. 31, p. 3131-3150.
707 Rogers, D.B., and Dreiss, S.J., 1995b, Saline Groundwater in Mono Basin, California:
708 2. Long-Term Control of Lake Salinity by Groundwater: Water Resources
709 Research, v. 31, p. 3151-3169.
710 Rogerson, M., Pedley, H., Kelham, A., and Wadhawan, J., 2014, Linking
711 Mineralisation Process and Sedimentary Product in Terrestrial Carbonates
712 Using a Solution Thermodynamic Approach: Earth Surface Dynamics, v. 2, p.
713 197-216.
714 Russell, I.C., 1889, Quaternary History of Mono Valley, California, US Government
715 Printing Office.

716 Saller, A., Rushton, S., Buambua, L., Inman, K., Mcneil, R., and Dickson, J.T., 2016,
717 Presalt Stratigraphy and Depositional Systems in the Kwanza Basin, Offshore
718 Angola: AAPG Bulletin, v. 100, p. 1135-1164.
719 Sanford, W.E., and Wood, W.W., 1991, Brine Evolution and Mineral Deposition in
720 Hydrologically Open Evaporite Basins.: Am. J. Sci., v. 291, p. 687–710.
721 Scholl, D.W., and Taft, W.H., 1964, Algae, Contributors to the Formation of Calcareous
722 Tufa, Mono Lake, California: Journal of Sedimentary Research, v. 34, p. 309-
723 319.
724 Scholl, D.W., Von Huene, R., St.-Amand, P., and Ridlon, J.B., 1967, Age and Origin of
725 Topography beneath Mono Lake, a Remnant Pleistocene Lake, California: GSA
726 Bulletin, v. 78, p. 583-600.
727 Selleck, B.W., Carr, P.F., and Jones, B.G., 2007, A Review and Synthesis of Glendonites
728 (Pseudomorphs after Ikaite) with New Data: Assessing Applicability as
729 Recorders of Ancient Coldwater Conditions: Journal of Sedimentary Research,
730 v. 77, p. 980-991.
731 Shearman, D.J., Mcgugan, A., Stein, C., and Smith, A.J., 1989, Ikaite, Caco3. 6h20,
732 Precursor of the Thinolites in the Quaternary Tufas and Tufa Mounds of the
733 Lahontan and Mono Lake Basins, Western United States: GSA Bulletin, v. 101,
734 p. 913-917.
735 Smithson, T., Carroll, R., Panchen, A., and Andrews, S., 1993, Westlothiana Lizziae
736 from the Viséan of East Kirkton, West Lothian, Scotland, and the Amniote
737 Stem: Earth and Environmental Science Transactions of The Royal Society of
738 Edinburgh, v. 84, p. 383-412.
739 Snæbjörnsdóttir, S.Ó., Gislason, S.R., Galeczka, I.M., and Oelkers, E.H., 2018,
740 Reaction Path Modelling of in-Situ Mineralisation of Co2 at the Carbfix Site at
741 Hellisheidi, Sw-Iceland: Geochimica et Cosmochimica Acta, v. 220, p. 348-366.

742 Souza-Egipsy, V., Wierzchos, J., Ascaso, C., and Nealson, K.H., 2005, Mg-Silica
743 Precipitation in Fossilization Mechanisms of Sand Tufa Endolithic Microbial
744 Community, Mono Lake (California): Chemical Geology, v. 217, p. 77-87.
745 Stine, S., 1990, Late Holocene Fluctuations of Mono Lake, Eastern California:
746 Palaeogeography, Palaeoclimatology, Palaeoecology, v. 78, p. 333-381.
747 Stine, S., 1991, Geomorphic, Geographic, and Hydrographic Basis for Resolving the
748 Mono Lake Controversy: Environmental Geology, v. 17, p. 67-83.
749 Stine, S., 2011, Late Holocene Volcanism in and Adjacent to Mono Lake, California:
750 2011 GSA Annual Meeting in Minneapolis.
751 Sutter, B., Mcadam, A.C., Mahaffy, P.R., Ming, D.W., Edgett, K.S., Rampe, E.B.,
752 Eigenbrode, J.L., Franz, H.B., Freissinet, C., Grotzinger, J.P., Steele, A., House,
753 C.H., Archer, P.D., Malespin, C.A., Navarro-González, R., Stern, J.C., Bell, J.F.,
754 Calef, F.J., Gellert, R., Glavin, D.P., Thompson, L.M., and Yen, A.S., 2017,
755 Evolved Gas Analyses of Sedimentary Rocks and Eolian Sediment in Gale
756 Crater, Mars: Results of the Curiosity Rover's Sample Analysis at Mars
757 Instrument from Yellowknife Bay to the Namib Dune: Journal of Geophysical
758 Research: Planets, v. 122, p. 2574-2609.
759 Tomascak, P.B., Hemming, N.G., and Hemming, S.R., 2003, The Lithium Isotopic
760 Composition of Waters of the Mono Basin, California: Geochimica et
761 Cosmochimica Acta, v. 67, p. 601-611.
762 Vidal, J., Macintyre, S., Mcphee-Shaw, E.E., Shaw, W.J., and Monismith, S.G., 2013,
763 Temporal and Spatial Variability of the Internal Wave Field in a Lake with
764 Complex Morphometry.: Limnology and Oceanography, v. 58, p. 1557-1580.
765 Wang, X., Ali, G., Hemming, S., Zimmerman, S., Stine, S., and Hemming, G., 2014,
766 Lake Level Changes in the Mono Basin During the Last Deglacial Period: AGU
767 Fall Meeting Abstracts.

768 Williams, G., 1997, Hot Springs of the Eastern Sierra, Tree by the River.
769 Wolthers, M., Nehrke, G., Gustafsson, J.P., and Van Cappellen, P., 2012, Calcite
770 Growth Kinetics: Modeling the Effect of Solution Stoichiometry: Geochimica Et
771 Cosmochimica Acta, v. 77, p. 121-134.
772 Wood, W.W., and Sanford, W.E., 1990, Ground-Water Control of Evaporite
773 Deposition: Economic Geology, v. 85, p. 1226-1235.
774 Zimmerman, S.H., Hemming, S.R., Kent, D.V., and Searle, S.Y., 2006, Revised
775 Chronology for Late Pleistocene Mono Lake Sediments Based on Paleointensity
776 Correlation to the Global Reference Curve: Earth and Planetary Science Letters,
777 v. 252, p. 94-106.

778

Captions

Table 1

Trace element concentrations of waters found in and around Mono Lake, California, in October 2014, After Brasier et al (2018).

Fig 1

Location of data collection a: location of Mono Lake within North America. B: position of measurements within Mono Lake. Bathymetry locations in red. Location of Scholl Terrace shown as purple (min) and brown (max); c: location of seismic lines and CTD casts Area 1; d: location of seismic lines and CTD casts in Area 2. Catchment size and stream-flow given in italics for each major creek. Non-gauged flow is estimated at 4.32×10^7 m^3 yr^{-1}. Catchment and stream-flow values taken from Mono Basin Environmental Impact Report 1993 (https://www.monobasinresearch.org/onlinereports/mbeir.php). The Rush Creek values here include the tributary Parker and Walker Creeks.

Fig 2

Bathymetry data collected in the Area 1. The section deepens to the north and shows tufa columns distributed throughout.

Fig 3

Bathymetry data collected in the Area2. a: details of columns at north of section; b: break of slope in centre of region.

803

804

805 Fig 4

806 Seismic data measured Area 1 (for location see Figure 1c). a: Line-001 b: Line-002;

807 c: Line-003.

808

809 Fig 5. Seismic data for Area 1 (for location see Figure 1c). Line-006, inflections marked

810 with green dashed line and numbered.

811

812 Fig 6

813 Seismic data measured in Area 2 (for locations see Figure 1c), a: Line-007, measured

814 north-south; b: Line2-007, measured south-north; c: Line2-008, measured south-

815 north.

816

817 Fig. 7. Seismic data measured in Area 2 (for locations see Figure 1d). Line2-009,

818 transecting line measuring north-south, inflections marked with green dashed line and

819 numbered.

820

821 Fig 8

822 Data obtained from CTD casts (for locations see Figure 1). a: Sound velocity v depth;

823 b: Temperature v depth; c: Conductivity; d: Temperature v Conductivity.

824

825 Fig 9

826 Comparison of, a: column height and depth and b: column height and column width in

827 both bathymetric sections.

828

829 Fig. 10

830 Gauged flow in Lee Vining Creek at Rhinedollar Dam (USGS gauging site 10287770)
831 from 1/10/1987 to 30/9/2020. Accessed on 23/8/21. All data is marked as “Approved”
832 on the USGS online database.

833 Figure 11

834 A) Sub-lacustrine tufa formation is explained by the mixing of calcium-rich meteoric
835 waters with carbonate-rich saline lake waters. This process is conditioned by the
836 location of the pycnocline which determines the lake depth where mixing takes place.
837 High saline and denser lake waters can infiltrate throughout deep seated lake faults
838 limiting the formation of tufa columns in the lake bottom.

839

Figure 1

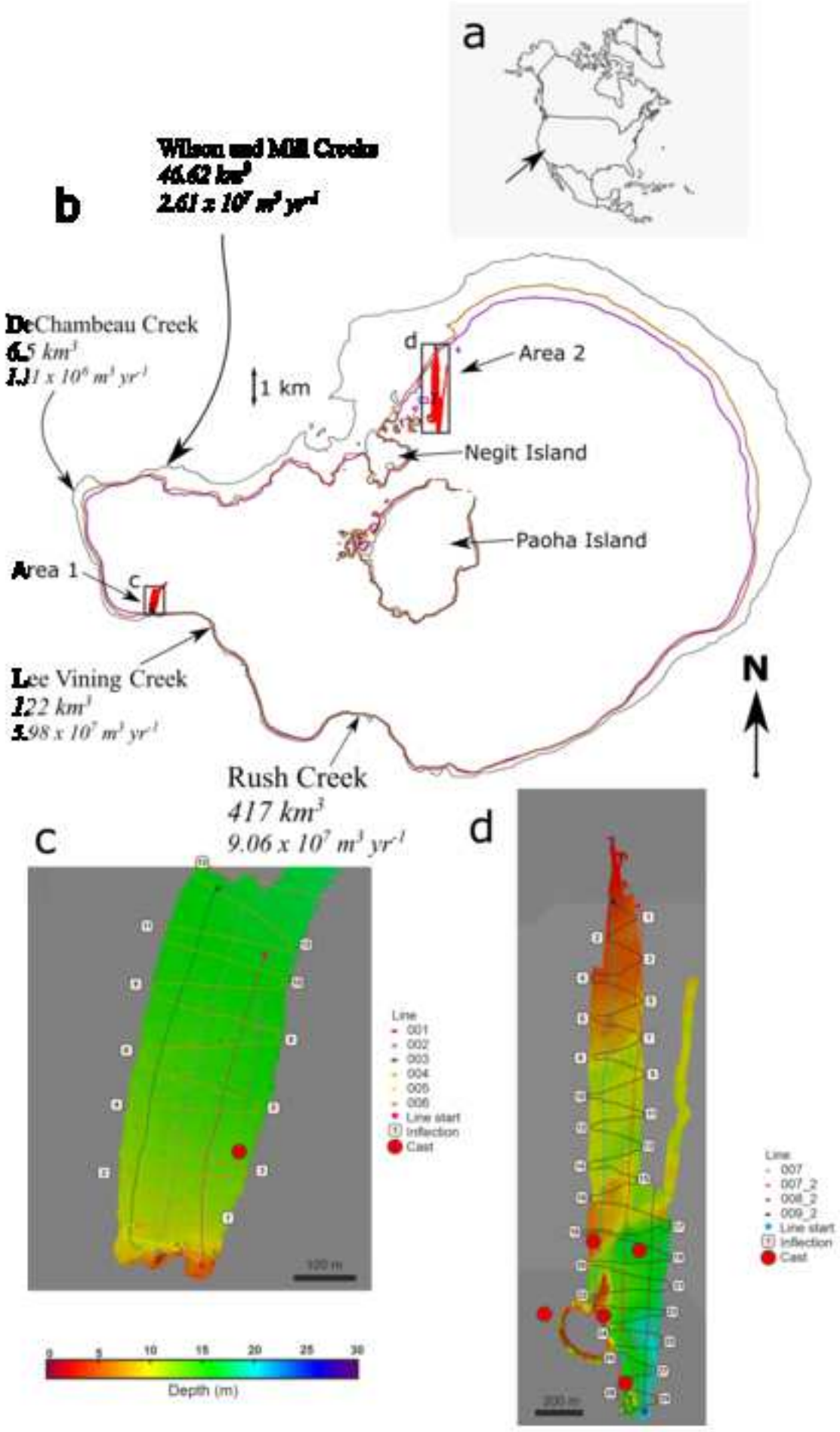

Figure 2

Click here to access/download;Figure;figure 2 small.png

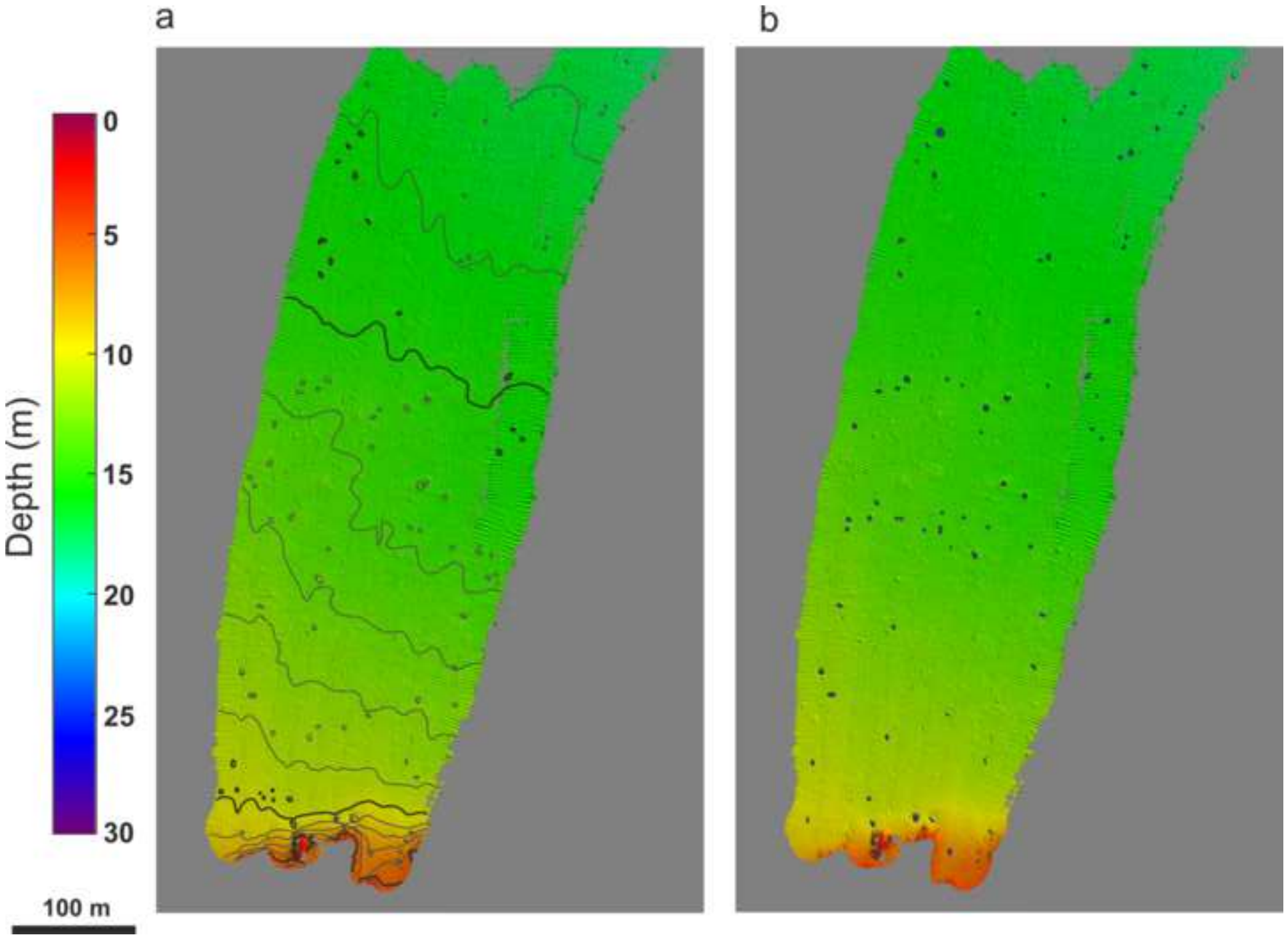

Figure 3

Click here to access/download;Figure;Figure3.png

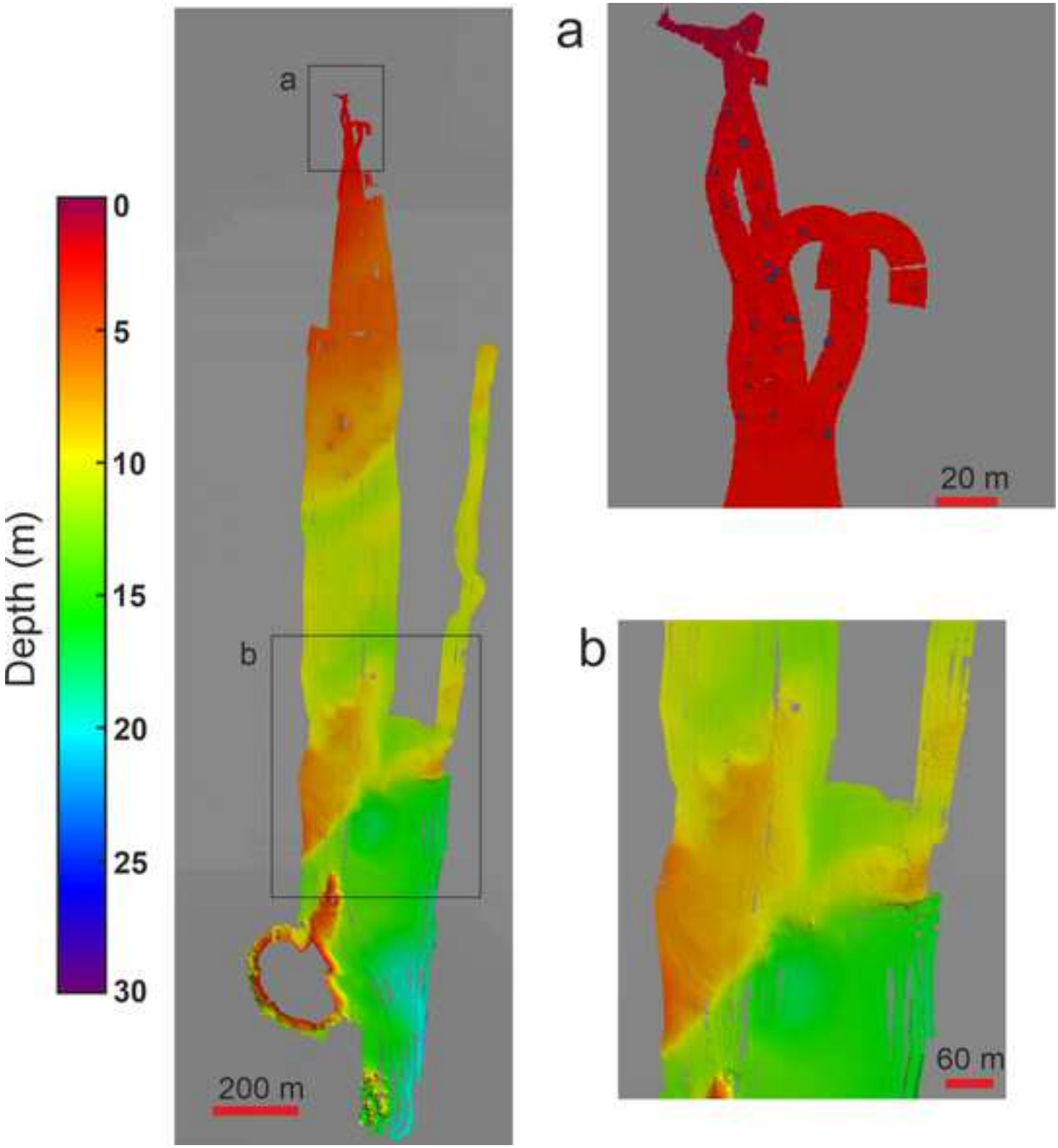

Figure 4

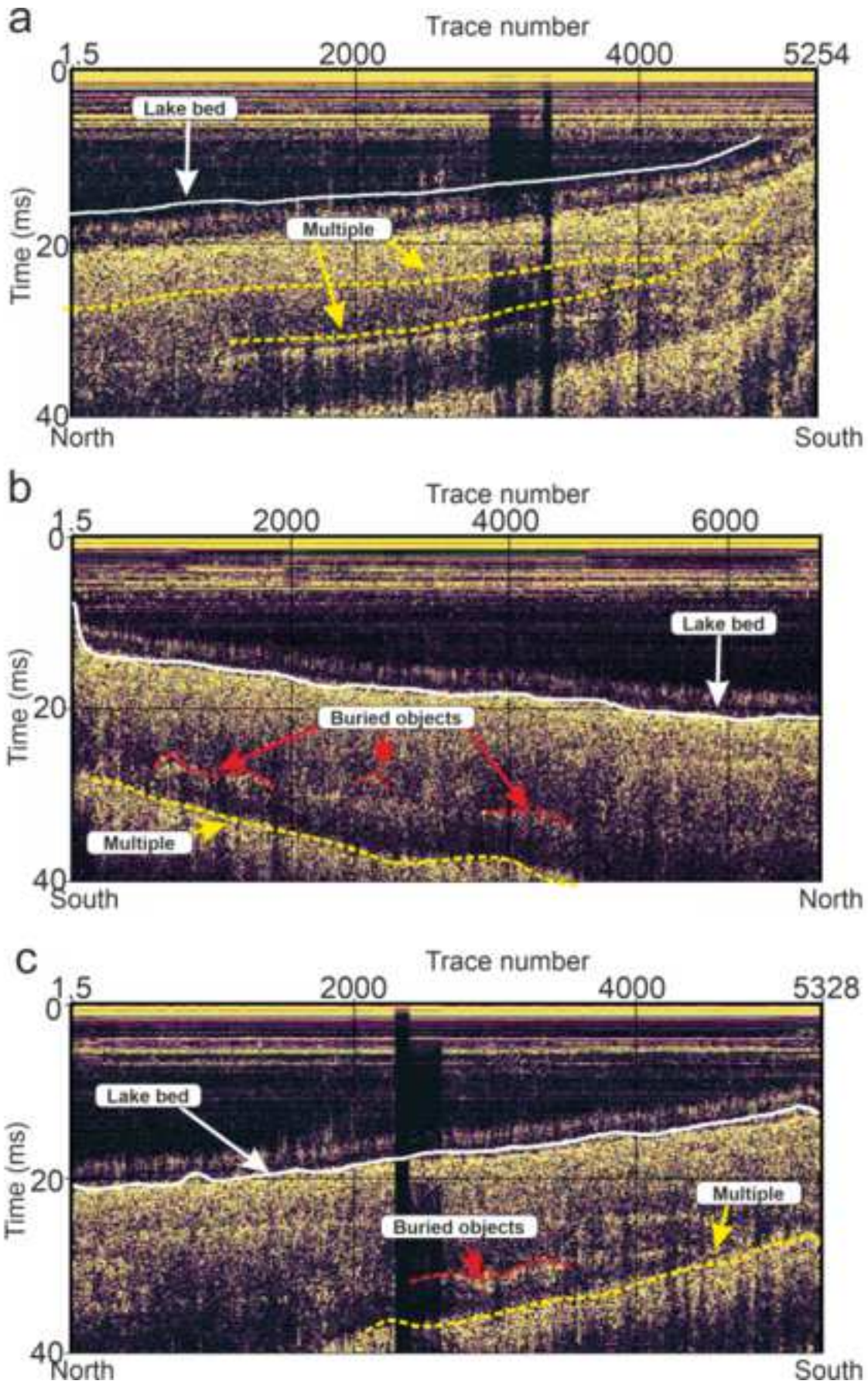

Figure 5

Click here to access/download;Figure;Figure 5.png

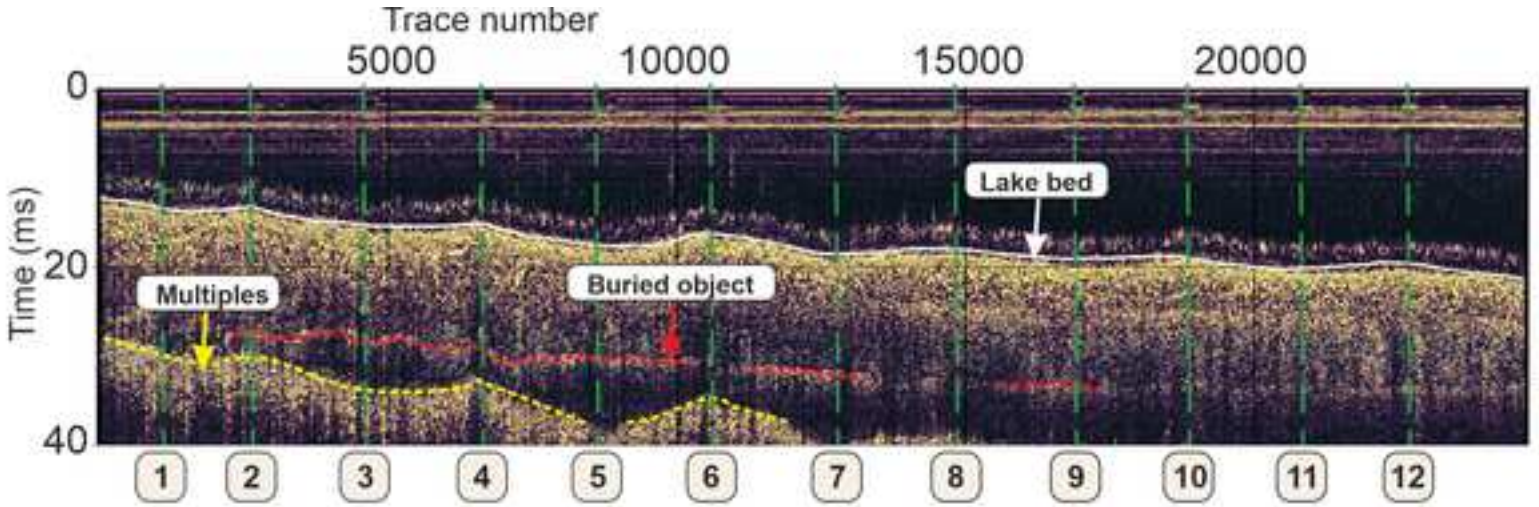

Figure 6

Click here to access/download;Figure;fig 6 smallest.png

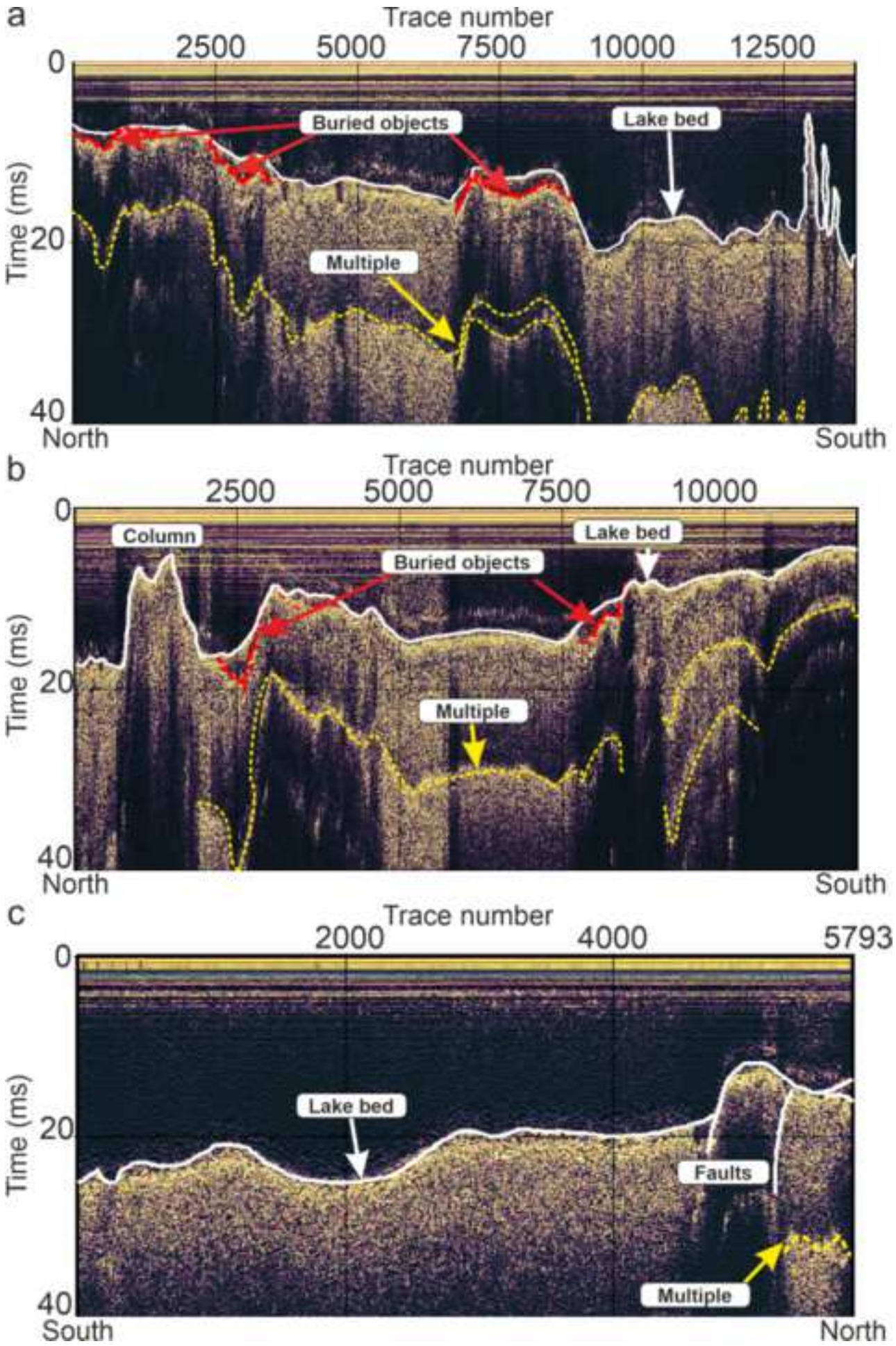

Figure 7

Click here to access/download;Figure;Figure 7.png

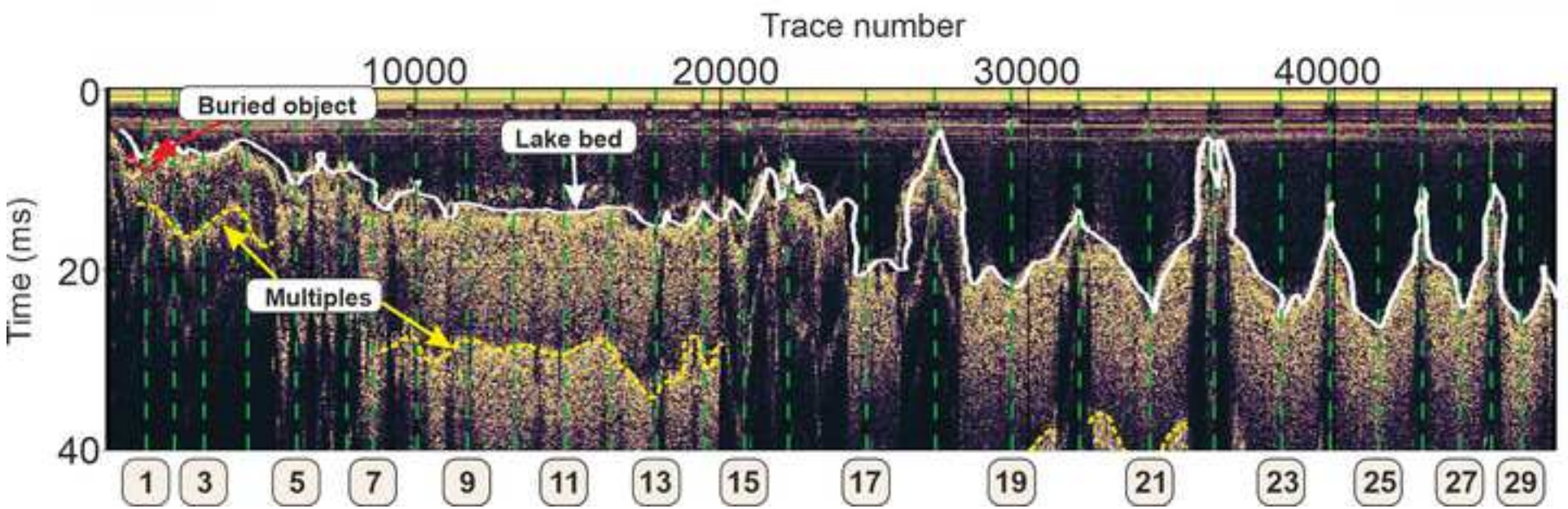

Figure 8

Click here to access/download;Figure;Figure 8.png

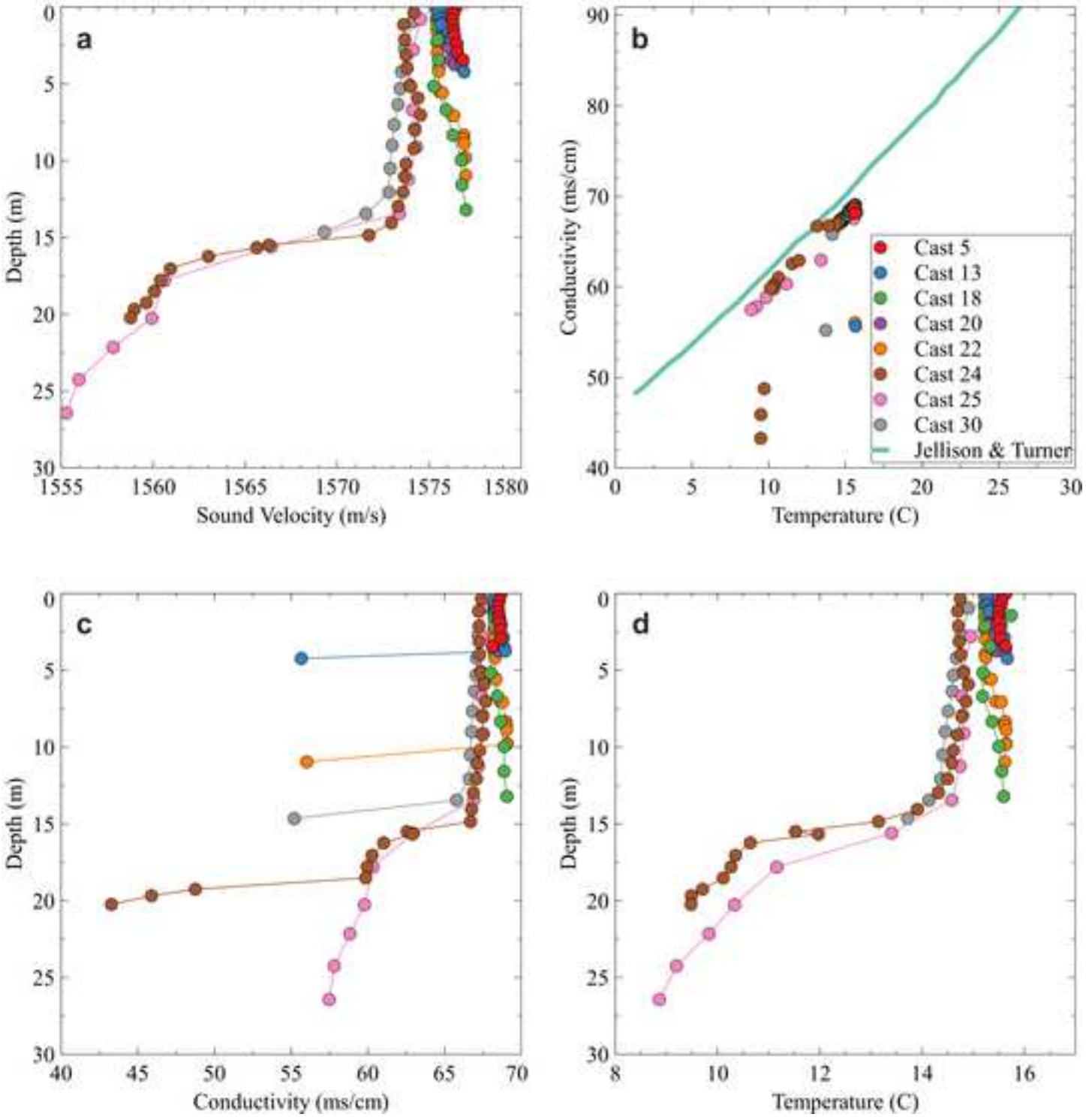

Figure 9

Click here to access/download;Figure;Figure9.png

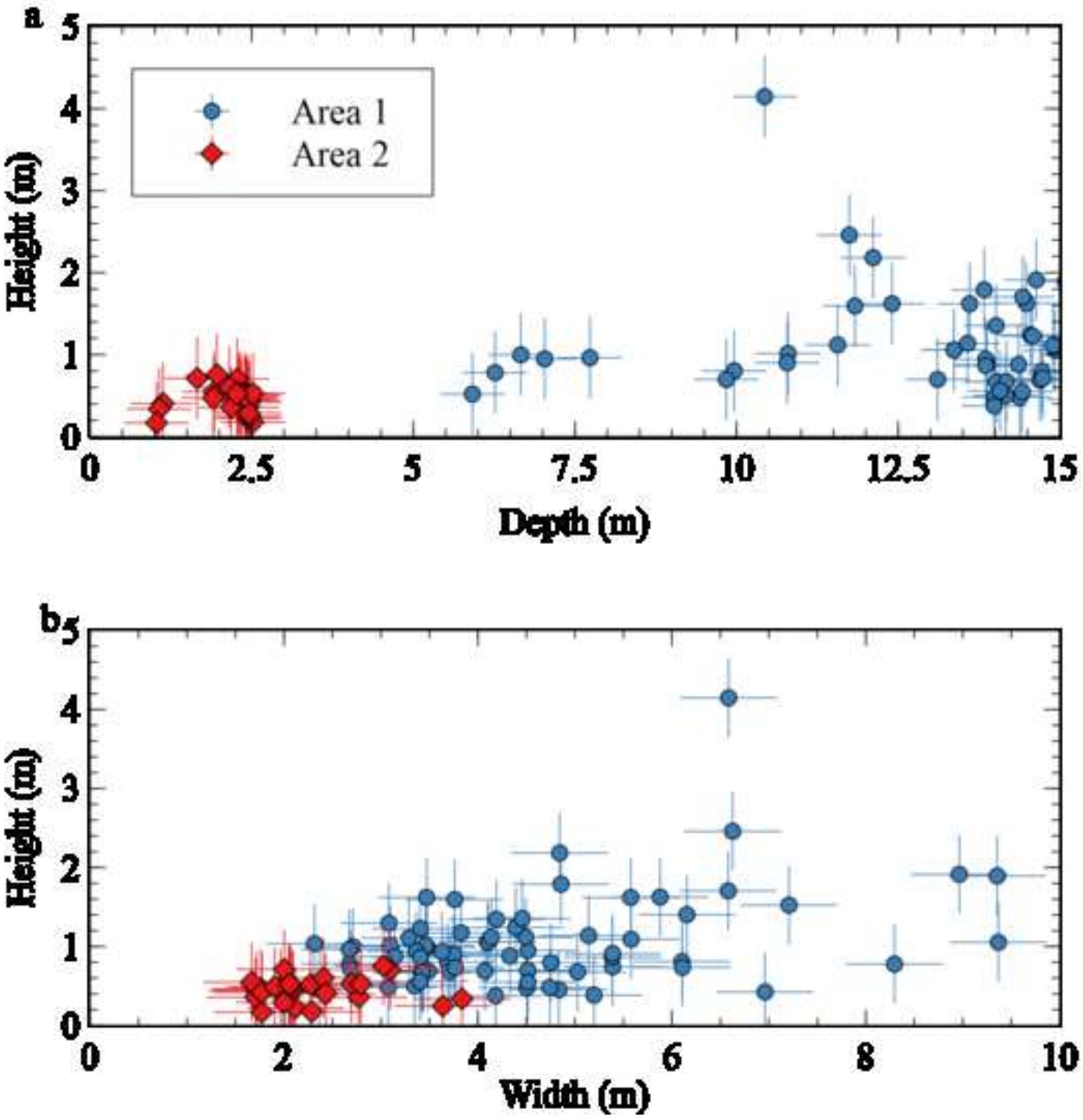

Figure 10

Click here to access/download;Figure;fig 10.jpg

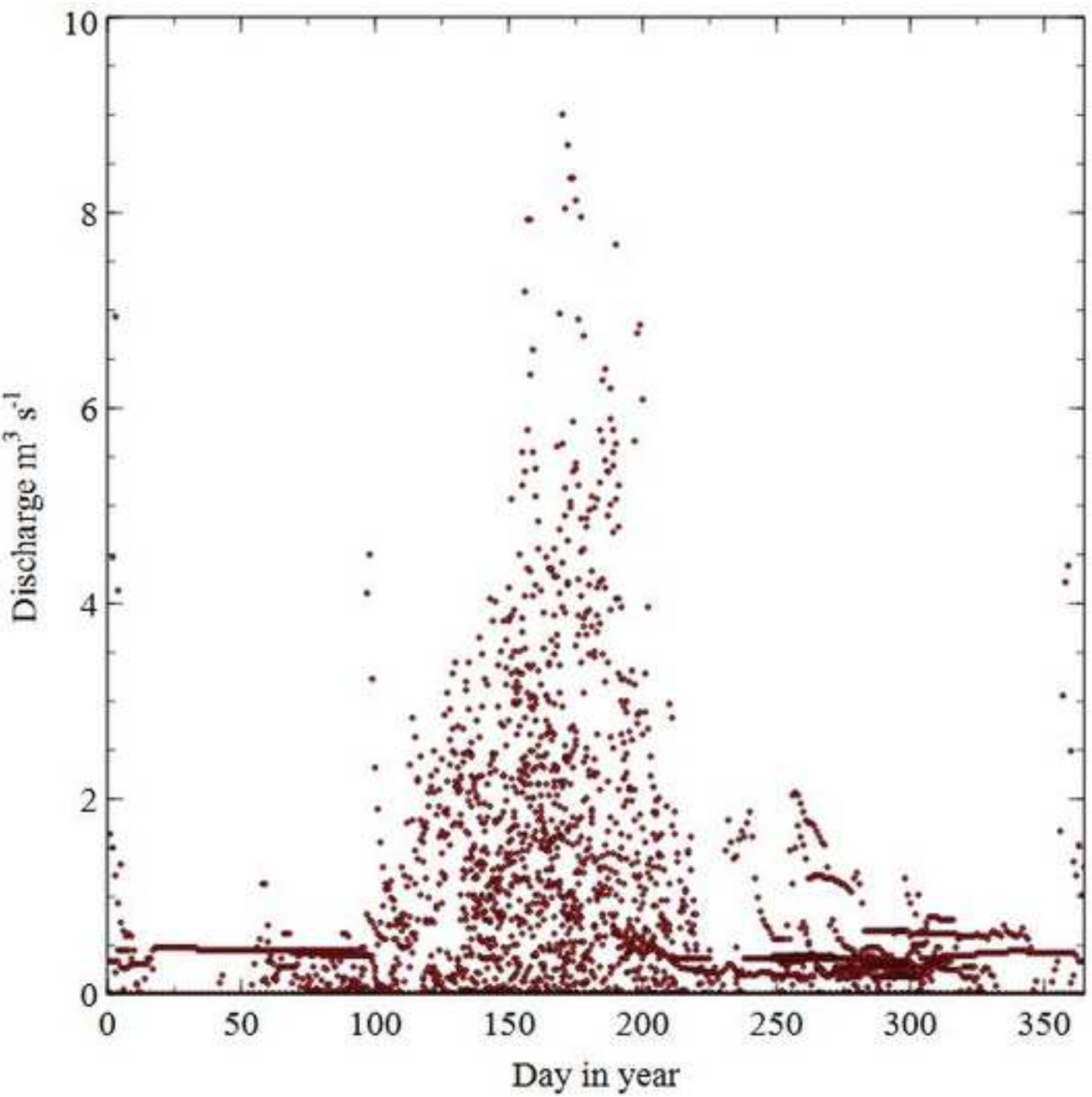

Figure 11

Click here to access/download;Figure;Ramon model fig_MR.pdf

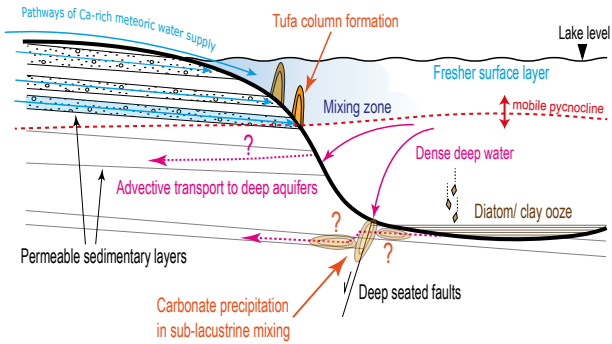

Table

Table 1: Trace element concentrations of waters found in and around Mono Lake, California, in October 2014, After Brasier et al (2018).

Site	Al	Ba	Ca	Cu	Fe	K	Li	Mg	Mn	S	Si	Sr
Mono Launch spring	0.084	0.001	2.238	0.002	0.036	17.584	0.254	0.587	0.001	17.976	5.272	0.005
Mono Lake 1	0.046	0.007	3.025	0.004	0.065	1383.753	11.653	12.585	0.011	1704.602	5.092	0.017
Mono Lake 2	0.198	0.008	3.378	0.005	0.066	1461.272	12.069	12.946	0.012	1659.955	4.995	0.021
Mono Lake 3	0.174	0.007	3.316	0.003	0.064	1434.739	11.855	12.861	0.012	1656.138	4.917	0.021
Simon Spring 3	0.034	0.016	22.401	0.000	0.045	7.964	0.221	22.580	0.005	3.974	18.253	0.173
Simon Spring 2	0.249	0.027	32.969	0.003	0.467	2.442	0.136	18.714	0.064	2.577	19.282	0.190
Mill Creek	0.116	0.021	8.526	0.011	0.226	3.466	0.000	0.857	0.011	3.843	3.093	0.038
Dechambeau Hot spring	0.019	0.010	11.567	0.002	0.041	6.860	0.232	2.460	0.016	31.326	18.269	0.162
Lee Vining Creek	0.046	0.011	7.916	0.004	0.124	0.964	0.000	0.565	0.007	2.171	2.308	0.040
Naval Beach spring	0.070	0.372	86.349	0.003	1.178	29.358	2.237	57.634	1.070	12.326	32.437	0.473
Rush creek	0.025	0.006	6.707	0.002	0.101	0.567	0.000	0.655	0.005	1.618	2.011	0.030
South Tufa lakeside Spring	0.031	0.292	111.943	0.000	8.462	32.005	1.441	45.901	1.994	15.698	31.001	0.537
Warm spring near Dechambeau	0.075	0.022	17.041	0.003	0.187	2.017	0.000	0.680	0.022	4.265	1.397	0.052